Magnetic properties of the spin-1 chain compound NiCl$_3$C$_6$H$_5$CH$_2$CH$_2$NH$_3$

F. Lipps[1], A.H. Arkenbout[2], A. Polyakov[2], M. Günther[3], T. Salikhov[4], E. Vavilova[4], H.-H. Klauss[3], B. Büchner[1,3], T.M. Palstra[2], and V. Kataev[1]

[1]*Leibniz Institute for Solid State and Materials Research IFW Dresden, D-01171 Dresden, Germany*

[2]*Zernike Institute for Advanced Materials, University of Groningen,*
Nijenborgh 4, 9747 AG Groningen, The Netherlands

[3]*Institut für Festkörperphysik, TU Dresden, D-01069 Dresden, Germany*

[4]*Kazan E.K. Zavoisky Physical Technical Institute of RAS, 420029 Kazan, Russia*

E-mail: v.kataev@ifw-dresden.de

We report experimental results of the static magnetization, ESR and NMR spectroscopic measurements of the Ni-hybrid compound NiCl$_3$C$_6$H$_5$CH$_2$CH$_2$NH$_3$. In this material NiCl$_3$ octahedra are structurally arranged in chains along the crystallographic *a* axis. According to the static susceptibility and ESR data Ni^{2+} spins $S = 1$ are isotropic and are coupled antiferromagnetically (AFM) along the chain with the exchange constant $J = 25.5$ K. These are important prerequisites for the realization of the so-called Haldane spin-1 chain with the spin-singlet ground state and a quantum spin gap. However, experimental results evidence AFM order at $T_N \approx 10$ K presumably due to small interchain couplings. Interestingly, frequency-, magnetic field-, and temperature-dependent ESR measurements, as well as the NMR data, reveal signatures which could presumably indicate an inhomogeneous ground state of co-existent mesoscopically spatially separated AFM ordered and spin-singlet state regions similar to the situation observed before in some spin-diluted Haldane magnets.

1. Introduction

Investigations of quantum magnetic phenomena in spin networks with reduced spatial dimensions of magnetic interactions is a well established and exciting field of research in condensed matter physics (for reviews see, e.g., Refs. 1–4). In systems with reduced dimensionality quantum effects become more relevant and ground states can be established not observed in three-dimensional systems. Ground state properties and excitation spectra depend critically on the dimensionality of the interaction, the dimensionality of the spin and the interplay between different interactions. On the experimental side, the search for realizations of the spin systems where magnetic exchange between the localized spins is restricted to one (1D) or two (2D) spatial dimensions is important for the verification of modern theories of quantum magnetism and for the exploration of novel magnetic phenomena.

Indeed, in many naturally occurring or man made solids the magnetic interactions are restricted to less than their three dimensions. This is the case when the crystal structure assembles in such a way that the couplings between spins along certain directions are much stronger than along others. There are 2D systems in which interaction takes place predominantly between magnetic ions arranged in a plane. In other systems magnetic ions are arranged in 1D structures, forming so-called spin chains.

One of the important classes of spin chains is the Haldane chain. This is a one-dimensional Heisenberg chain with integer spins and antiferromagnetic (AFM) nearest-neighbor coupling. Haldane predicted that the ground state

of such a system would be a nonmagnetic singlet state which would be separated in energy from the excited triplet state by a gap Δ [5]. This gap is not an anisotropy gap, but is due to the quantum nature of the $S = 1$ system. Haldane considered the pure Heisenberg Hamiltonian for an easy-axis-configuration [5]. In order to explore the limits of the Haldane phase bi-quadratic exchange and single-ion anisotropy, among other parameters, can be taken into account. Already those simple extensions reveal rich physics involved in the quasi-one-dimensional antiferromagnetic integer Heisenberg spin chains. A general Hamiltonian of the Haldane system is given in [6]:

$$\mathcal{H} = J\sum_i [\mathbf{S}_i \mathbf{S}_{i+1} + \beta(\mathbf{S}_i \mathbf{S}_{i+1})^2] +$$
$$+ \sum_i [D(S_i^z)^2 - g\mu_B S_i^\alpha H^\alpha]. \quad (1)$$

Here J is the energy coupling constant between neighboring spins $\mathbf{S}$. β describes the bi-quadratic exchange. Uniaxial single-ion anisotropy is considered: With z being the chain direction either easy axis (spin along the chain, $D < 0$) or easy plane (spin perpendicular to the chain, $D > 0$) is favored. The interaction with a magnetic field H is described by the typical Zeeman term where g is the g-factor and μ_B is the Bohr magneton.

Besides the bi-quadratic exchange the single-ion anisotropy plays a crucial role for the realization of a Haldane system. The energy gap Δ between the singlet ground state $|0\rangle$ and the excited triplet state $|1\rangle$ directly depends on the value of D. The gap is largest for the absence of single-ion anisotropy, but an energy difference exists within a certain range of D. For $D > J$ an anisotropy gap opens.

The first material discovered to realize the Haldane system was $Ni(C_2H_8N_2)_2–NO_2ClO_4$ (NENP) [7]. Similar to the system studied in this present work NENP contains the transition element Ni realizing the chain structure in an organic matrix. NENP exhibits a single-ion anisotropy [7], which results in the splitting of the excited triplet state [8] and with that an anisotropic Haldane gap. However the ground state is still the singlet state. Since then a number of other compounds featuring Ni-based chains have been discovered and investigated (for details see, e.g., Refs. 6, 9).

In the present paper which summarizes some of the results of the PhD work in Ref. 10 we report the magnetic properties of the inorganic-organic hybrid compound with the chemical formula $NiCl_3C_6H_5CH_2CH_2NH_3$ as revealed by static magnetic measurements, and ESR and NMR local probe techniques. This compound contains structurally well isolated Ni chains where Ni^{2+} spins $S = 1$ are coupled antiferromagnetically with the isotropic exchange coupling constant $J = 25.5$ K. Despite showing typical signatures of the 1D AFM behavior in the static susceptibility and ESR at elevated temperatures, the Ni-hybrid compound

orders AFM at $T_N \approx 10$ K. The occurrence of the magnetically ordered ground state and not of the expected Haldane spin-singlet state might be presumably related to the presence of residual interchain magnetic couplings. Still, the ESR and NMR data indicate a possible competition between these two different states which could be speculatively interpreted in terms of the spatially inhomogeneous ground state with coexisting AFM order and the Haldane state in the same sample. We speculate that such an inhomogenous ground state, that was observed before in some spin-diluted Haldane magnets, could be a consequence of a small structural disorder that promotes coupled AFM-ordered clusters around the defects in the spin chains which are intertwined with the chain segments still exhibiting a Haldane gap.

2. Experimental details

Samples of the Ni-hybrid compound $NiCl_3C_6H_5CH_2CH_2NH_3$ were grown in ethanol solution and consist of an anorganic backbone of Ni atoms in the octahedral environment of six chlorine atoms. The general synthesis procedure and primary characterizations are described in [11]. The Ni–Ni distance can be subtly varied by choosing different organic constituents [12]. The crystallographic structure is shown in Fig. 1. An almost perfectly symmetric octahedron is realized, with the angle between Cl–Ni–Cl found to be $\beta_1 \approx 86°$ and $\beta_2 \approx 94°$. For Ni–Cl–Ni the angle is about $\gamma \approx 75°$. Along the c direction the individual Ni chains are separated by a large organic complex consisting of a benzene structure with an amino group connected to it by two carbon atoms. In the b direction the NiCl-octahedra are separated directly through hydrogen bonds between chloride and the amino group.

Static magnetization was measured with a VSM-SQUID magnetometer from Quantum Design Inc. which allows measurements in the temperature range from 1.8 to 325 K, in magnetic fields up to 7 T. ESR measurements with a microwave frequency of 9.6 GHz and fields up to 0.9 T were performed using a standard Bruker EMX X-band
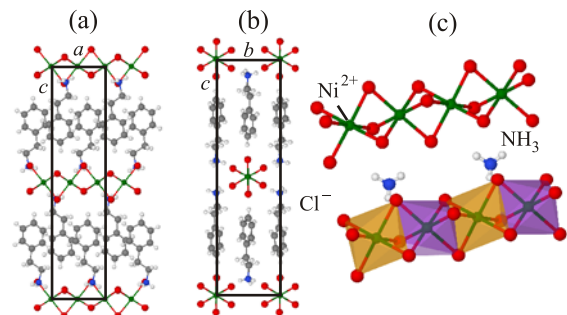

Fig. 1. (Color online) Crystallographic structure of the Ni-hybrid $NiCl_3C_6H_5CH_2CH_2NH_3$. Shown are the view on the ac plane (a), bc plane (b) and a close-up (c) of two chains where the face-sharing octahedra are highlighted.

spectrometer. It is equipped with an ESR 900 He-flow-cryostat from Oxford Instruments, which allows measurements at variable temperatures between 3.6 and 300 K. High-field/high-frequency ESR (HF-ESR) was measured using a homemade spectrometer which is described in detail elsewhere [13]. In the latter set-up a superconducting magnet from Oxford Instruments can generate static magnetic fields up to 16 T while a variable temperature insert enables measurements between 1.6 and 300 K. For the generation and detection of microwaves with frequencies up to 360 GHz a vector network analyzer from ABmm was used. ESR measurements were performed with resonant cavities at frequencies of 9.6, 50, 83 and 93 GHz on single crystals of the Ni-hybrid and at frequencies up to 360 GHz on a powder sample. For the measurements at 9.6 GHz, several single crystals were aligned on a teflon bar to increase the signal/noise ratio. ^{35}Cl NMR experiments in a temperature range 1.5 K $< T <$ 150 K were performed with conventional pulse NMR techniques using a Tecmag LapNMR spectrometer and a 16 T field-sweep superconducting magnet from Oxford Instruments. The polycrystalline powder was placed in a glass tube inside a Cu coil with a frequency of the resonant circuits of 41 MHz. The spectra were collected by point-by-point sweeping of the magnetic field and integration of the Hahn spin echo at each field step. The nuclear spin-lattice relaxation rate was measured with the saturation recovery method.

3. Experimental results and discussion

3.1. Susceptibility and magnetization

Static susceptibility χ of the powder Ni-hybrid sample as a function of temperature at an external magnetic field of 0.01 T is shown in Fig. 2. $\chi(T)$ increases with decreasing temperature and shows a broad peak with a maximum around 30 K. The susceptibility then decreases down to about 10 K. This is the expected behavior for a one-dimensional spin system. Indeed, as can be seen in Fig. 1, Ni atoms enclosed in an octahedron of oxygen or chlorine are usually in the Ni^{2+} 3d^8 configuration with an effective spin moment of $S = 1$ [14]. The intra-chain coupling between Ni(II)-ions is mediated by the surrounding Cl atoms of the face sharing octahedra. The angle of $\gamma \approx 75°$ indicates an overlap of the Cl orbitals, thus an AFM superexchange is expected for the Ni ions along the chain. Thus, from the structural point of view alone, this system seems to be a promising candidate for a Haldane system.

For a magnetically isotropic 1D system with AFM coupling the Weng equation [15] for the susceptibility of isotropic $S = 1$ ring systems can be used to fit the temperature dependence of the static susceptibility [16]:

$$\chi_{S=1} = \frac{N\beta^2 g^2}{k_B T} \frac{2 + 0.019\alpha + 0.777\alpha^2}{3 + 4.346\alpha + 3.232\alpha^2 + 5.834\alpha^3} \quad (2)$$
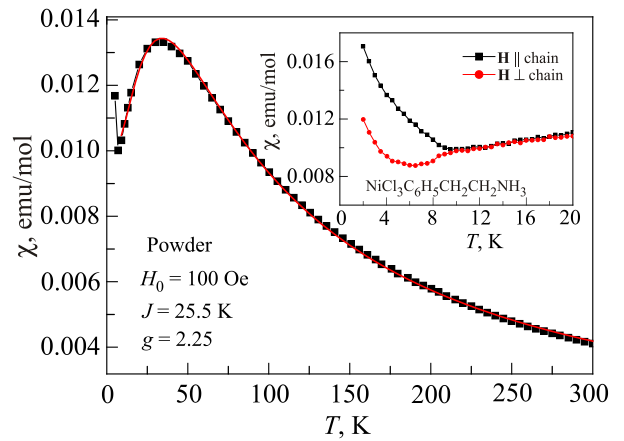

Fig. 2. Static susceptibility as a function of temperature. A broad maximum around $T \approx 25$ K is visible. Inset shows the low-temperature susceptibility measured on single crystals with magnetic field parallel and perpendicular to the chain direction.

with $\alpha = J/(k_B T)$, k_B is the Boltzmann constant, and N is the number of spins. For the fit to the static susceptibility data (Fig. 2), the g factor was kept fixed with $g = 2.25$ (see ESR results below) and no temperature independent offset χ_0 was assumed. The equation reproduces well the static susceptibility. From the fit an exchange constant of $J = 25.5$ K is extracted. For a Heisenberg spin chain with integer spin moment $S = 1$ a Haldane gap system is predicted. In the absence of single-ion anisotropy the Haldane gap is maximal and can be calculated from the exchange constant as $\Delta_H = 0.411J$ [6]. With $J = 25.5$ K a Haldane gap of $\Delta_H = 10.5$ K is expected.

In a Haldane system the ground state is a nonmagnetic singlet state. Therefore the susceptibility should go to zero with decreasing temperature. The static susceptibility indeed decreases down to temperatures around 10 K, but below that temperature a minimum is visible followed by an increase in the static susceptibility with decreasing temperatures (Fig. 2).

Susceptibility measurements on single crystals reveal that the $\chi(T)$ is isotropic down to about 10 K. Below that temperature, the static susceptibility shows a minimum and an anisotropic increase, different for the magnetic field applied along the chain direction and perpendicular to it (Fig. 2, inset). A Curie-like increase in the susceptibility is often associated with paramagnetic impurities present in the sample. Susceptibility from impurities could dominate over the vanishing susceptibility of a Haldane system. However, this cannot explain the anisotropy observed.

The magnetization as a function of applied magnetic field was determined at temperatures of 1.8, 8, 11 and 15 K up to 7 T (Fig. 3). While at a temperature of 15 K the magnetization increases linearly with the applied field, at 1.8 K it shows a nonlinear behavior with an inflection point at about 3.5 T. This is clearly visible in the derivative of the magnetization in Fig. 3(b). For the intermediate tempera-
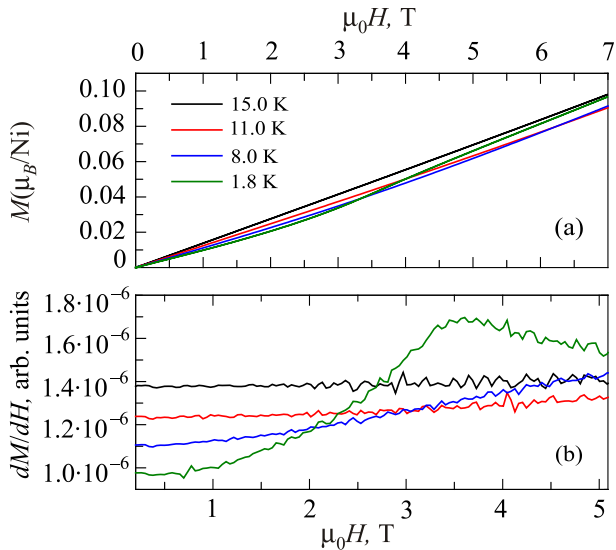
Fig. 3. (Color online) Magnetic field dependences of the magnetization (a) and its derivative *dM/dH* (b) on powder sample. For *T* = = 15 K a linear increase in the magnetization with magnetic field is observed. At the lowest temperature a spin-reorientation is visible.

tures deviations from the linear increase can already be observed, but the effect is drastically reduced. Such an inflection is usually associated with a spin-flop transition of a magnetically ordered antiferromagnetic system, i.e., a reorientation of spins in the increasing external field. This points to an AFM ordering.

An AFM ordering is also consistent with the susceptibility data at low temperatures. For the easy axis of an antiferromagnet the susceptibility should go to zero, while for the easy plane it should stay constant with decreasing temperature. The susceptibility measured on the single crystals can be interpreted as a sum of that of an antiferromagnetic state and that of paramagnetic impurities. The direction perpendicular to the chain is the easy axis of the system. Note here that the Haldane system Pb(Ni$_{1-x}$Mg$_x$)$_2$V$_2$O$_8$ orders antiferromagnetically, upon substitutional doping of Ni with Mg ($S = 0$ impurities). In contrast to the investigations in this work, the Curie tail observed in the susceptibility of doped PbNi$_2$V$_2$O$_8$ is suppressed at the onset of AFM order [17]. This indicates that in the Ni-hybrid compound (not all) impurities are involved in the magnetic ordering.

The total magnetization is quite small with $M \approx 0.1 \mu_B$/Ni at the maximum field of 7 T. For the Ni^{2+} ions contributing to the magnetization a saturation field of $M_{\text{sat}} = gS =$ $= 2.25 (\mu_B$/Ni) is expected. This is consistent with one-dimensional Heisenberg AFM as well as Haldane systems, in which the saturation magnetization can often not be reached even in fields up to 40 T [17,18].

Altogether, the results of static susceptibility and magnetization on the Ni-hybrid samples indicate a one-dimensional spin chain which exhibits an antiferromagnetically ordered ground state that develops below

$T_N \approx 10$ K with the easy axis perpendicular to the chain direction and a spin-flop transition at $H_c = 3.5$ T. A certain amount of impurities is present in the sample.

3.2. Electron spin resonance

To get a more detailed picture about the physics of the Ni-hybrid spin chain compound ESR measurements were conducted. ESR is a valuable tool to probe the local static and dynamic magnetic properties which also can give information about the different energy states in one-dimensional Heisenberg antiferromagnets [8,19–23]. A single-crystalline ESR spectrum at 9.6 GHz (X-band) at $T = 25$ K is shown in Fig. 4 (inset) for external magnetic fields applied along the chain direction and perpendicular to it. The resonance signal exhibits a Lorentzian line around a resonance field of about 0.3 T corresponding to a *g* factor of $g = 2.25$. This *g* factor is typical for a Ni^{2+} ion in an octahedral crystal field [14]. The ESR signals are almost perfectly isotropic over the whole temperature range down to about 8 K. This indicates the absence of single-ion anisotropy [$D = 0$ in Eq. (1)] in the Ni-hybrid compound meaning that an isotropic Heisenberg spin chain is realized in the paramagnetic state which is very favorable for the realization of a Haldane system. The absence of single-ion anisotropy is most likely related to the regular octahedral ligand coordination of Ni^{2+}. In such high symmetry of the ligand crystal field the $S = 1$ state of Ni^{2+} remains 3-fold degenerate in zero magnetic field implying the isotropic character of the Ni spin [14]. The integrated intensity I_{ESR} of an ESR signal is determined by the intrinsic susceptibility χ_{spin} of the spins participating in the resonance [14]. From Lorentzian fits of the ESR signals of the Ni-hybrid sample $I_{ESR} \propto \chi_{\text{spin}}$ can be evaluated and the temperature dependence of χ_{spin} is plotted in Fig. 4. The spin susceptibility shows a maximum around 20 K with a sharp
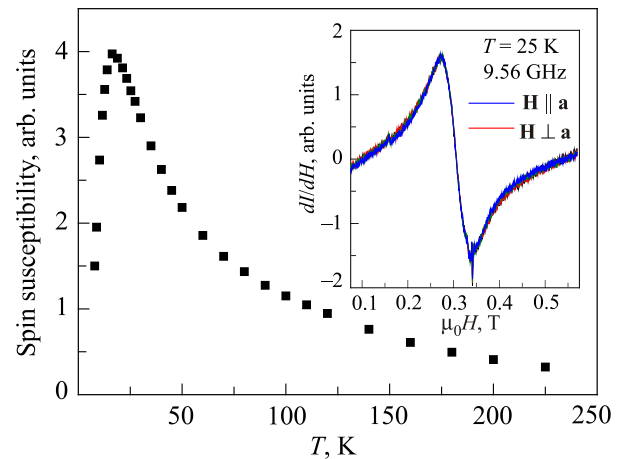

Fig. 4. (Color online) Temperature dependence of the spin susceptibility as determined from ESR measurements around 9.56 GHz. Inset shows the ESR spectra (absorption derivative) at $T = 25$ K for magnetic fields applied parallel and perpendicular to the chain direction.

decrease at the low-temperature side. This decrease is associated with the broadening and the strong decrease in the amplitude of the resonance. It is clearly visible that, in comparison to the bulk static susceptibility (Fig. 2), the spin susceptibility exhibits an enhanced maximum and a steeper decrease when going to lower temperatures. From Fig. 4 it is apparent that towards zero temperature χ_{spin} would approach the zero value. Below 8 K the signal cannot be observed at this frequency. This clear tendency towards zero spin susceptibility indicates that the Ni spin system (giving rise to this spectrum) seems to behave as a Haldane system down to 8 K. This is in contrast to the observed magnetic order at $T_N \approx 10$ K in the static susceptibility and magnetization measurements.

However, there can be other spin subsystems present which cannot be observed by ESR at frequencies around 10 GHz. Especially ESR resonances associated with the AFM ordering which was detected by susceptibility and magnetization measurements may occur outside of the field and the frequency ranges of the X-band spectrometer. Thus, HF-ESR experiments at higher frequencies and higher magnetic fields were performed as well.

Similar to the X-band results, at all higher probing frequencies up to 360 GHz a single isotropic line is observed for temperatures above 10 K. Figure 5 shows the ESR spectra at a frequency of about 93 GHz for selected temperatures between 20 and 2.5 K measured on one single crystal. ESR spectra with the magnetic field perpendicular to the chain direction are shown in Fig. 5(a). At 20 K only a single Lorentzian line is visible, in agreement with the experiments at 10 GHz. With decreasing temperature this line decreases in intensity and shifts to lower fields. Interestingly, two additional lines appear at fields of about 1 and 5 T and become stronger in intensity with decreasing temperatures. This is a new feature not observed at lower frequencies.
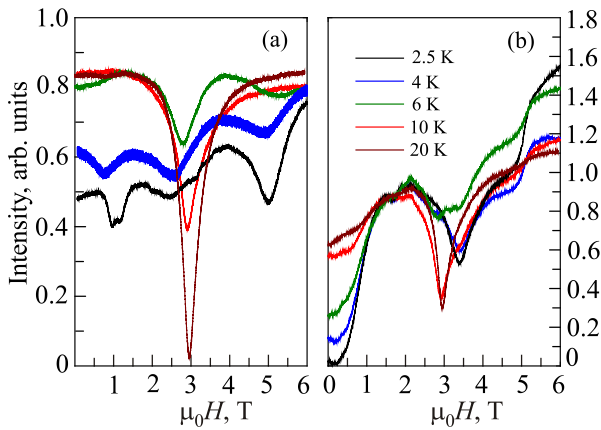

Fig. 5. (Color online) ESR spectra at 93 GHz with magnetic field perpendicular to the chain (a) and along the chain (b) for temperatures from 20 K down to 2.5 K. While the central line decreases additional lines develop with decreasing temperature.

For the magnetic field parallel to the chain [Fig. 5(b)], the central line also decreases, but shifts to higher fields. At almost zero magnetic field another signal appears. However it is not clear if the minimum of the spectrum is fully visible. That is why the absolute value of the resonance field extracted cannot be very accurate. At around 5 T another feature is observed which appears phase-shifted with respect to the central line. This probably does not originate from the main crystal and could be a spurious effect due to some fragment at another position in the resonator.

The above discussed ESR signals from single crystals of the Ni-hybrid compound measured with the resonator-based setups at 10–93 GHz as well as data for a powder sample measured without resonators at higher frequencies up to 360 GHz are summarized in a frequency ν vs magnetic field H chart in Fig. 6. The paramagnetic signals at temperatures above 10 K follow a linear dependence $\nu = (g\mu_B/h)H$ (dashed line) with the slope given by the g factor $g = 2.25$. Here h is the Plank constant. The theoretical equations [24,25] for resonances of a collinear two-sublattice antiferromagnet are shown by solid curves (for **H** ∥ easy axis) and by a dash-dot line (for **H** ⊥ easy axis):

H ∥ easy axis, $H < H_c$:

$$\nu_{1,2} = \Delta_a \pm \frac{g\mu_B}{h}H\,; \qquad (3)$$

H ∥ easy axis, $H > H_c$:

$$\nu_1 = 0, \quad \nu_2 = \sqrt{\left(\frac{g\mu_B}{h}H\right)^2 - \Delta_a^2}\,; \qquad (4)$$

H ⊥ easy axis:

$$\nu = \sqrt{\left(\frac{g\mu_B}{h}H\right)^2 + \Delta_a^2}\,, \qquad (5)$$

where $g = 2.25$ and the so-called magnetic anisotropy gap at zero field $\Delta_a = (g\mu_B/h)H_c$ with $\mu_0 H_c = 3.5$ T being the spin-flop magnetic field value obtained from magnetization measurements.

As known from the susceptibility measurements on the single crystal the easy axis is perpendicular to the chain. The side peaks at 93 GHz for this direction [Fig. 5(a)] roughly agree with the theoretical AFM resonance modes (Fig. 6). A similar assignment can be made for the ESR signals for **H** ∥ chain axis as the hard-direction AFM modes. For a powder sample, modes for both directions are present due to the powder averaging. Notably, the signals at all measured frequencies that follow the paramagnetic resonance branch lose their intensity below ~20 K as if they corresponded to some excited magnetic state that gets thermally less populated with decreasing temperature. These signals are still detectable below $T_N \approx 10$ K where their position shifts as if the resonating spins sensed the internal magnetic fields caused by the antiferromagnetic order in their vicinity.
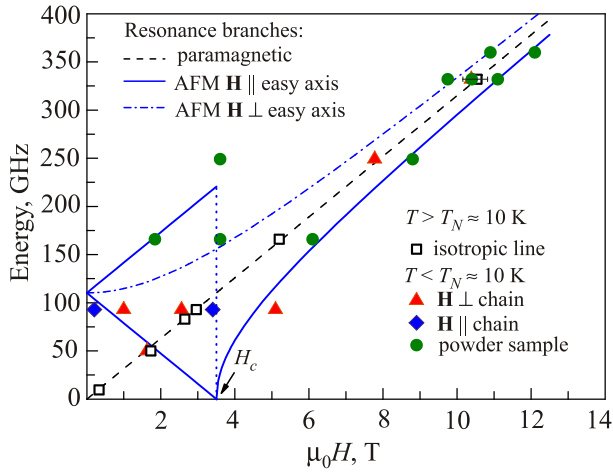
Fig. 6. (Color online) Summary of the ESR modes in the frequency vs magnetic field plot. Open squares correspond to the isotropic ESR signals observed in the paramagnetic regime at $T > 10$ K. Triangles and diamonds denote the ESR modes detected at $T < T_N \approx$ ≈ 10 K for the external field applied perpendicular and parallel to the Ni-chain axis, respectively. Circles depict the signals of a powder sample at $T < T_N \approx 10$ K. Dash line corresponds to the paramagnetic branch $\nu = (g\mu_B/h)H$, and the solid and dash-dot curves represent the AFM branches for the easy- and the hard directions of a collinear two-sublattice antiferromagnet according to Eqs. (3), (4) and Eq. (5), respectively. H_c denotes the spin-flop field determined by the magnetization measurements. Note that the signals grouped around the paramagnetic branch strongly decrease in intensity below ~ 20 K, whereas the signals grouped around the AFM branches appear first below $T_N \approx 10$ K and grow in intensity at lower temperatures.

Based on the ESR results, one could conjecture that in the studied Ni-hybrid compound two spin subsystems could be realized, the one which orders AFM at $T_N \approx 10$ K, and the other one which shows signatures of thermally activated paramagnetism. It is tempting to speculate that the latter subsystem might develop the Haldane spin gap and could be spatially separated but yet still coupled to the AFM ordered subsystem.

Indeed, a coexistence between singlet quantum ground state and classically ordered magnetic state was reported, e.g., for the Haldane compound PbNi$_2$V$_2$O$_8$ where the spinless defects were introduced in the Ni-spin chain by Mg doping [17,21]. The development of the AFM order was attributed to the nucleation of the soliton-like AFM clusters around the defect sites in the Haldane chain which couple together due to residual interchain magnetic exchange. ESR experiments have indicated that at small concentration of defects Pb(Ni$_{1-x}$Mg$_x$)$_2$V$_2$O$_8$ ($x \le 0.02$) develops a spatially inhomogeneous state of co-existing large AFM ordered clusters, small paramagnetic clusters, and spin-singlet Haldane regions [21].

The Ni-hybrid compound studied in the present work was not doped intentionally with nonmagnetic defects.

However, it is conceivable that there might be some (small) structural disorder in the crystals, resulting in a segmentation of the Ni-chains in fragments of different length. At the chain ends uncompensated spins and/or AFM correlated regions could develop and interact with each other, and be responsible for the small Curie-like upturns of the static susceptibility at low temperatures and AFM order at $T_N \approx 10$ K, as evidenced by the static magnetic and ESR measurements. On the other hand, one cannot completely exclude the possibility that still a certain amount of Ni-chains in the sample develop the Haldane spin-singlet ground state which could explain the thermally activated paramagnetic ESR signals which are detected on the background of the AFM resonance modes.

Finally, it should be noted that ESR spectra were observed in Haldane systems, which were attributed to singlet-triplet transitions between the $S = 0$ ground state and the $S = 1$ triplet state in NENP [20,26]. These transitions are forbidden by the dipole selection rules. However, mixing between pure $S = 0$ and $S = 1$ spin states is possible through anisotropic exchange interactions or single-ion anisotropy. Then the forbidden transitions can be observed in an ESR experiment. For the Ni-hybrid compound ESR data in the paramagnetic state evidence the absence of single-ion anisotropy ($D = 0$). Therefore it is likely that the mixing is too small to make an observation of the forbidden transitions possible.

3.3. NMR spectroscopy

Additional insights into the local magnetic properties and the spin dynamics of the Ni-hybrid compound were obtained by ^{35}Cl NMR spectroscopy. The NMR spectrum has a total width of more than 2 T and consists of two structured peaks corresponding to two isotopes of ^{35}Cl and ^{37}Cl and a quadrupole background. The temperature evolution of the main line for ^{35}Cl nuclei below a temperature of 50 K is shown in Fig. 7(a). The "two-horn" shape of the spectrum is present approximately down to 30 K, transforming with a further temperature decrease into the three peaks structure where the additional central line shifts gradually to higher fields towards the Larmor field. The second isotope ^{37}Cl line undergoes the same changes. Below 10 K, the shape of the spectrum changes dramatically: the signals identified above as the main lines for both Cl isotopes disappear, and the total width of the spectrum increases by approximately 1 T already at $T = 8$ K. Such a sharp transformation of the NMR spectrum suggests the occurrence of the antiferromagnetic transition around 9 K, consistent with the Néel temperature $T_N \approx 10$ K determined by the static magnetization measurements. The temperature dependence of the nuclear relaxation rate T_1^{-1} [Fig. 7(c)] measured at the midpoint of the spectrum exhibits a broad maximum around 35 K similar to the behavior of the static susceptibility. At $T_N \approx 10$ K the temperature dependence has a weak maximum while with a further temperature
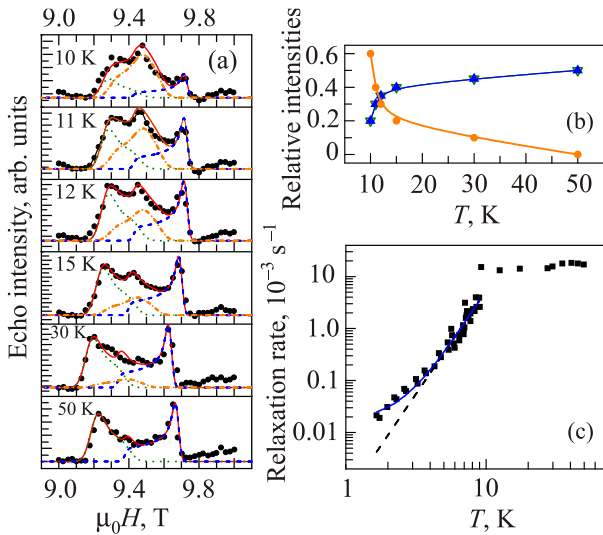
Fig. 7. (Color online) (a) Selected ^{35}Cl NMR spectra (solid circles) in the temperature range 10 K < T < 50 K. Solid line represents a modelling of the three-component powder averaged spectra, dash, dot and dash-dot lines show different spectral contributions (see the text); (b) Temperature dependence of the relative intensities of the central spectral contribution (solid circles) and of the left and right side spectral contributions [almost coinciding up (blue) and down (green) triangles]; (c) Temperature dependence of the ^{35}Cl nuclear spin-lattice relaxation T_1^{-1} (solid squares). Dash line represents a fit by the power law $\sim T^{3.89}$, solid line shows a sum of the power law $\sim T^{4.13}$ and of the activation law $\sim \exp(-3.2/T)$ (see the text).

decrease the relaxation rate drops sharply. A sharp change in the temperature dependence at 10 K indicates a possible phase transition at this temperature, again in agreement with the static data, while the absence of a pronounced maximum, which is typical for establishing the magnetic order in 3D systems, suggests the magnetic quasi-one-dimensionality of the Ni-hybrid compound.

The NMR measurements were performed in fields of the order of 9 T. In such fields, the hypothetical Haldane gap, which value at $H = 0$ is estimated theoretically as 10.5 K, is expected to be almost closed due to the lowering of the energy of the $S_z = |-1\rangle$ state of the excited $S = 1$ triplet. We attempted to describe the transformation of the powder spectra near the Néel temperature as a result of the change of the symmetry of the local fields acting on the Cl nuclei due to the development of the Ni spin correlations in the chain. Though no perfect fit to the experimental spectra could be achieved, the reasonable agreement between the model and experiment requires an assumption of the appearance and growth of an additional component with a different symmetry which is located between the components of the high-temperature spectrum [Fig. 7(a)]. The appearance of this signal can be speculatively explained assuming a phase separation in the chains into the regions where the growth of AFM correlations leads to the ordering and the regions where the Haldane nonmagnetic state could still develop

with decreasing temperature. The magnitude and symmetry of the field at the Cl nuclei in the "Haldane-like" part of the chains is determined by nearest magnetic regions, and the intensity of this NMR signal increases with decreasing temperature. Concomitantly, the intensity of the left and right signals originating from the paramagnetic regions falls down [Fig. 7(b)] despite increasing their width. Another possible origin of this mid-signal in the NMR spectrum could be the Cl nuclei near the chain defects, the response from which becomes more pronounced when the Ni spins in the chains begin to correlate. Also the behavior of the relaxation rate $T_1^{-1}(T)$ suggests a situation more complex than a simple AFM ordering model. In the AFM ordered state, $T_1^{-1}(T)$ is mainly driven by magnon scattering, leading to a power-law temperature dependence [17,18]. In the limit where the temperature is much higher than the anisotropy gap in the spin-wave spectrum, $T_1^{-1}(T)$ either follows a T^3 dependence due to a two-magnon Raman process or a T^5 dependence due to a three-magnon process. If the temperature is smaller than the gap, the relaxation rate is proportional to $T^2 \exp(-\Delta_a/k_B T)$ where Δ_a is the spin-wave anisotropy gap. In the Ni-hybrid compound the relaxation below 10 K does not obey this combined power-exponential law. The temperature dependence can be well described by the $\sim T^{3.89}$ power law down to ~ 3 K suggesting that the relaxation is mainly governed by the two-magnon process [Fig. 7(c)]. However, in order to fit also the low-temperature part of the $T_1^{-1}(T)$ dependence, we need to add the second term, which has an activation character with a gap of about 3.2 K [Fig. 7(c)]. In this case the first term is proportional to $T^{4.13}$ suggesting that the relaxation is likely governed mainly by the three-magnon process. If this gap is a conjectured Haldane gap, its value of 3.2 K would be presumably a bit too large for such a high field of the measurement. Nevertheless, within the speculative phase separation scenario one would indeed expect that just below T_N the nuclear spin relaxation is determined by regions with a Néel order. As the temperature is lowered, this relaxation channel strongly slows down and the contribution from the "Haldane-like" regions becomes noticeable.

4. Conclusions

In summary, we have studied magnetic properties of the Ni-hybrid compound $NiCl_3C_6H_5CH_2CH_2NH_3$ by static magnetic as well as ESR and NMR measurements. In this material structurally well-defined Ni spin-1 antiferromagnetic chains are realized. ESR data in the paramagnetic state at elevated temperatures evidence an isotropic Heisenberg character of the Ni spins. The analysis of the temperature dependence of the static susceptibility yields an AFM intra-chain exchange interaction constant $J = 25.5$ K. Though the above results suggest this Ni-hybrid compound as a possible realization of the Haldane spin-1 AFM chain that should develop a singlet ground state with the quan-

tum spin gap $\Delta_H = 0.411J = 10.5$ K, experimental data show that this material orders AFM at $T_N \approx 10$ K and the excitations below T_N, as probed by NMR, are predominantly magnon-like. The AFM order and not the Haldane spin-singlet ground state is possibly due to the non-negligible interchain interactions. Interestingly, besides the AFM resonance modes detected at $T < T_N$, a thermally activated paramagnetic ESR signal is observed in the spectra measured at different frequencies. It could be compatible with the thermally activated signal of a Haldane chain. To explain this signal, as well as the unusual shape transformation of the ^{35}Cl NMR spectrum and the peculiar behavior of the nuclear spin relaxation rate, we speculate that a spatially inhomogeneous ground state might be realized in the Ni-hybrid compound. Assuming the occurrence of a small amount of structural defects in the Ni-chain that cut the spin chain in fragments of different length one could conjecture the nucleation of the soliton-like AFM clusters at the chain ends which couple together and order AFM. We further speculate that besides the ordered phase there might be mesoscopically spatially separated regions in the sample where the Ni-chains still exhibit a Haldane spin gap, similar to the situation which was reported for the spin-diluted Haldane magnet Pb(Ni$_{1-x}$Mg$_x$)$_2$V$_2$O$_8$.

1. *Magnetic Properties of Layered Transition Metal Compounds*, L.J. De Jongh (ed.), Kluwer Academic Publishers (1990).

2. H.-J. Mikeska and A. Kolezhuk, *Quantum Magnetism, Lect. Notes Phys.*, Vol. 645, U. Schollwöck, J. Richter, D.J. Farnell, and R. Bishop (eds.), Springer-Verlag, Berlin, Heidelberg (2004), p. 1.

3. S. Sachdev, *Nature Phys.* **4**, 173 (2008).

4. A.A. Zvyagin, *Quantum Theory of One-Dimensional Spin Systems*, Cambridge Scientific Publishers (2010).

5. F.D.M. Haldane, *Phys. Rev. Lett.* **50**, 1153 (1983).

6. M.V.J.P. Renard and L.P. Regnault, *Magnetism:Molecules to Materials — Models and Experiments*, M.D.J.S. Miller (ed.), Wiley-VCH (2001).

7. J.P. Renard, M. Verdaguer, L.P. Regnault, W.A.C. Erkelens, J. Rossat-Mignod, and W.G. Stirling, *Europhys. Lett.* **3**, 945 (1987).

8. M. Sieling, W. Palme, and B. Lüthi, *Z. Phys. B: Condens. Matter* **96**, 297 (1995).

9. K. Wierschem and P. Sengupta, *Modern Phys. Lett. B* **28**, 1430017 (2014).

10. F. Lipps, *Ph.D. Thesis*, Technical University Dresden (2011).

11. A. Arkenbout, *Ph.D. Thesis*, University of Groningen, Zernike Institute for Advanced Materials (2010).

12. A. Polyakov, *Ph.D. Thesis*, University of Groningen, Zernike Institute for Advanced Materials (2015).

13. C. Golze, A. Alfonsov, R. Klingeler, B. Büchner, V. Kataev, C. Mennerich, H.-H. Klauss, M. Goiran, J.-M. Broto, H. Rakoto, S. Demeshko, G. Leibeling, and F. Meyer, *Phys. Rev. B* **73**, 224403 (2006).

14. A. Abragam and B. Bleaney, *Electron Paramagnetic Resonance of Transition Ions*, Oxford University Press (1970).

15. C.Y. Weng, *Ph.D. Thesis*, Carnegie Institute of Technology (1968).

16. J. Ribas, M. Monfort, C. Diaz, C. Bastos, C. Mer, and X. Solans, *Inorg. Chem.* **34**, 4986 (1995).

17. I. Tsukada, K. Uchinokura, A. Zheludev, T. Hayashi, N. Miura, and P. Böni, *Phys. Rev. Lett.* **83**, 632 (1999).

18. T. Masuda, K. Uchinokura, T. Hayashi, and N. Miura, *Phys. Rev. B* **66**, 174416 (2002).

19. M. Hagiwara, K. Katsumata, I. Affleck, B.I. Halperin, and J.P. Renard, *Phys. Rev. Lett.* **65**, 3181 (1990).

20. I. Affleck, *Phys. Rev. B* **46**, 9002 (1992).

21. A.I. Smirnov, V.N. Glazkov, H.-A. Krug von Nidda, A. Loidl, L.N. Demianets, and A.Y. Shapiro, *Phys. Rev. B* **65**, 174422 (2002).

22. A.I. Smirnov, V.N. Glazkov, T. Kashiwagi, S. Kimura, M. Hagiwara, K. Kindo, A.Y. Shapiro, and L.N. Demianets, *Phys. Rev. B* **77**, 100401 (2008).

23. H.-A. Krug von Nidda, N. Büttgen, and A. Loidl, *Euro. Phys. J. — Special Topics* **180**, 161 (2009).

24. E.A. Turov, *Physical Properties of Magnetically Ordered Crystals*, Academic Press, New York and London (1965).

25. S. Foner, *Magnetism*, G. Rado and H. Suhl (eds.), Academic, New York (1963).

26. M. Date and K. Kindo, *Phys. Rev. Lett.* **65**, 1659 (1990).

27. M. Belesi, F. Borsa, and A.K. Powell, *Phys. Rev. B* **74**, 184408 (2006).

28. A. Yogi, N. Ahmed, R. Nath, A.A. Tsirlin, S. Kundu, A.V. Mahajan, J. Sichelschmidt, B. Roy, and Y. Furukawa, *Phys. Rev. B* **91**, 024413 (2015).